

Graph polyhedral divisions in growing cell aggregates

Urban Železnik,^{1,2} Matej Krajnc,² and Tanmoy Sarkar^{2,*}

¹*Faculty of Mathematics and Physics, University of Ljubljana, Jadranska 19, SI-1000 Ljubljana, Slovenia*

²*Jožef Stefan Institute, Jamova 39, SI-1000 Ljubljana, Slovenia*

(Dated: August 15, 2024)

In the recently proposed Graph Vertex Model (GVM), cellular rearrangements are implemented as local graph transformations of the cell aggregate, represented by a knowledge graph [1]. This study extends GVM to incorporate cell division, a critical biological process involved in morphogenesis, homeostasis, and disease progression. Like cellular rearrangements, cell division in GVM begins by identifying a subgraph of nodes and links, involved in the division, by matching suitable graph patterns or templates within the full knowledge graph. The matched subgraph is then transformed to incorporate topological changes within the knowledge graph, caused by the division event. Importantly, when this transformation is applied to a polygon in a 2D tiling, it performs the transformation, required to divide a polygon, indicating that the 3D graph transformation is general and applicable also to 2D vertex models. Our extension of GVM enables the study of the dynamics of growing cell aggregates in 3D to offer new insights into developmental processes and cancer growth.

INTRODUCTION

Space-filling packings play a fundamental role in shaping the structures and arrangements observed across diverse biological and physical systems. For instance, cells in many animal tissues are packed in a foam-like structure, whereby polygonal cell-cell contacts are arranged in a three-dimensional network and each cell is represented by a polyhedron. Just like in foams, cells in tissues dynamically exchange neighbors in response to local shear stresses. In space filling-polyhedral cell aggregates, these neighbor exchanges manifest as local topological transformations of the underlying network of cell-cell contacts [2–5].

In addition to cell-neighbor exchanges, common to foams and tissues, the network topology can change in tissues also through cell division, where a cell gets divided into two daughter cells (Fig. 1A). This process—which is not observed in foams [6]—plays a pivotal role in tissue morphogenesis and is subject to tight regulation, crucial for maintaining tissue homeostasis and ensuring the accurate development of shape, size, and patterns [7–11]. Disruption in this regulation can lead to developmental abnormalities and cancer [12]. A cell may divide symmetrically or asymmetrically, which significantly influences developmental processes, recovery after injury, and disease progression [13–15]. Therefore, unravelling the detailed process of performing a cell division and its influence on tissues may provide insights into developing effective cancer treatment and prevention strategies.

Computationally, cells in confluent tissues are often modeled as interacting geometric entities or fields [16]. Specifically, within the framework of the “standard” vertex model, a cell in three dimensions (3D) is represented by a polyhedron [17, 18]. However, due to complexities associated with the implementation of the vertex model, tissue mechanics have predominantly been

explored in 2D. A recently proposed approach Graph Vertex Model (GVM) addresses these complexities by proposing a new solution to implementing dynamical topological changes associated with cell rearrangements in a vertex model [1].

Like in the standard vertex model, GVM represents each cell by a polyhedron, parameterized by positions of its vertices, \mathbf{r}_i . A cell changes its shape by altering \mathbf{r}_i under the influence of mechanical forces, governed by a system of dynamical equations. Assuming a friction-dominated environment, the equation of motion for vertex i reads

$$\eta \frac{d\mathbf{r}_i}{dt} = -\nabla_i W + \mathbf{F}_i^{(a)}. \quad (1)$$

Here η is the friction coefficient, W is the potential energy of the aggregate, and $\mathbf{F}_i^{(a)}$ is the contribution from all active forces.

In the vertex model, the potential energy is typically written as a function of cells’ geometric properties, e.g., edge lengths, surface areas of polygons, cell volumes, etc. In order to compute these quantities and their gradients, vertex model needs to keep track of the connections between different geometric entities. In particular, a pair of vertices constitute an oriented edge \mathbf{e}_j , a series of edges constitute a polygon \mathbf{p}_k , and a series of polygons constitute a cell \mathbf{c}_l . Since edges are oriented, every edge contains a head- and a tail vertex. The information about the headness/tailness of vertices is given by a contextual property of vertices, $s \in \{-1, +1\}$ (-1 and $+1$ corresponding to tail and head vertices, respectively). Here, “contextual” refers to the fact that headness and tailness of a given vertex are not this vertex’s absolute properties, but rather properties that are bound to a specific edge of which the vertex is part of. In turn, every polygon is prescribed a normal vector and its orientation is defined by the right-hand rule. The

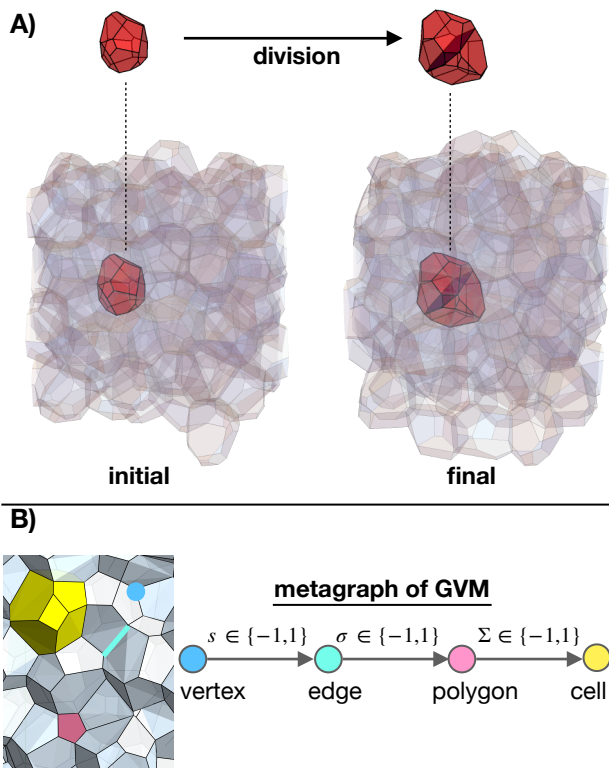


FIG. 1. **Two stages of cell division and the metagraph of GVM.** **A** A cell before and after cell division is marked in red color in the cell aggregate where the rest of the cells are colored in transparent shades. The marked cell in the initial stage (left) grows twice its regular size and divides into two daughter cells in the final stage (right). **B** On the left, typical vertex, edge, polygon and cell in an aggregate are shaded in blue, cyan, magenta and yellow color, respectively. On the right, the metagraph of GVM is depicted using same color code for nodes which are connected by directed arrows indicating strong hierarchy. Contextual properties or signs of vertex \rightarrow edge, edge \rightarrow polygon and polygon \rightarrow cell relationships are indicated by s , σ and Σ , respectively.

constituent edges of every polygon are prescribed a contextual property $\sigma \in \{-1, +1\}$ (-1 and $+1$ corresponding to edges pointing in polygon’s negative and positive direction, respectively). Similarly, constituent polygons of every cell are prescribed a contextual property $\Sigma \in \{-1, +1\}$ (-1 and $+1$ corresponding to the normal vectors of polygons pointing towards or away from the cell center, respectively). The most important step forward in GVM relative to the “standard” vertex model is its unique way of storing the topological relations between geometric elements (i.e., vertices, edges, polygons, and cells), described above. In particular, GVM’s data model is based on a knowledge graph, whose nodes represent the geometric elements, whereas the links between the nodes represent topological relationships between the elements (Fig 1B). The graph structure of the database

and its rules are summarized in the so-called metagraph, which describes in what way different nodes are allowed to be linked to each other. The metagraph of the GVM reads vertex \rightarrow edge \rightarrow polygon \rightarrow cell, where each arrow points from a hierarchically inferior to superior nodes (Fig 1B). This strong hierarchy among different types of nodes keeps all higher-order topological information without creating redundant data, which helps in the straightforward implementation of topological transformations in the cell network.

For instance, cell neighbor exchanges within a cell aggregate are performed by two primary transformations: reopening a vanishing edge into a triangle, known as Edge-to-Triangle transformation (ET), and creating an edge from a disappearing triangle, known as Triangle-to-Edge transformation (TE). These transformations are performed in the GVM by merely deleting and creating about a dozen relationships in the graph database [1]. The simplicity and straightforwardness of GVM motivate its extension to incorporate cell division which remains largely unexplored, especially in 3D.

Here, we implement cell division in the GVM framework. Like TE and ET transformations, cell division is performed by matching the initial subgraph representing the data that gets transformed during the division, and transforming this subgraph by deleting and creating relationships. The required graph transformation is uniquely defined for a division of any type of polyhedral cell into a pair of daughter cells. Significantly, similarly to cell rearrangements, the graph transformation needed to divide a cell within a 2D polygonal tiling is a subset of the full graph transformation representing the division of a polyhedron in 3D.

RESULTS

To illustrate all the steps of a cell division within GVM, we start with a simplified reduced-dimensionality 2D polygonal packing and in the subsequent sections, we expand the framework to 3D cell aggregates.

Cell division in 2D polygonal tiling

In a 2D polygonal tiling, each cell is represented by a polygon, i.e., polygon p_2 in the left panel of Fig. 2. After cell division, polygon p_2 splits in two daughter polygons p_1 and p_2 , which either have symmetric or asymmetric sizes, depending on the position and orientation of the division plane. This plane (line in 2D), denoted by e_5 in Fig. 2, intersects two edges of p_2 (i.e., edges e_1 and e_2 in Fig. 2).

The algorithm for dividing a cell begins by identifying two intersected edges of the dividing polygon p_2 . Next,

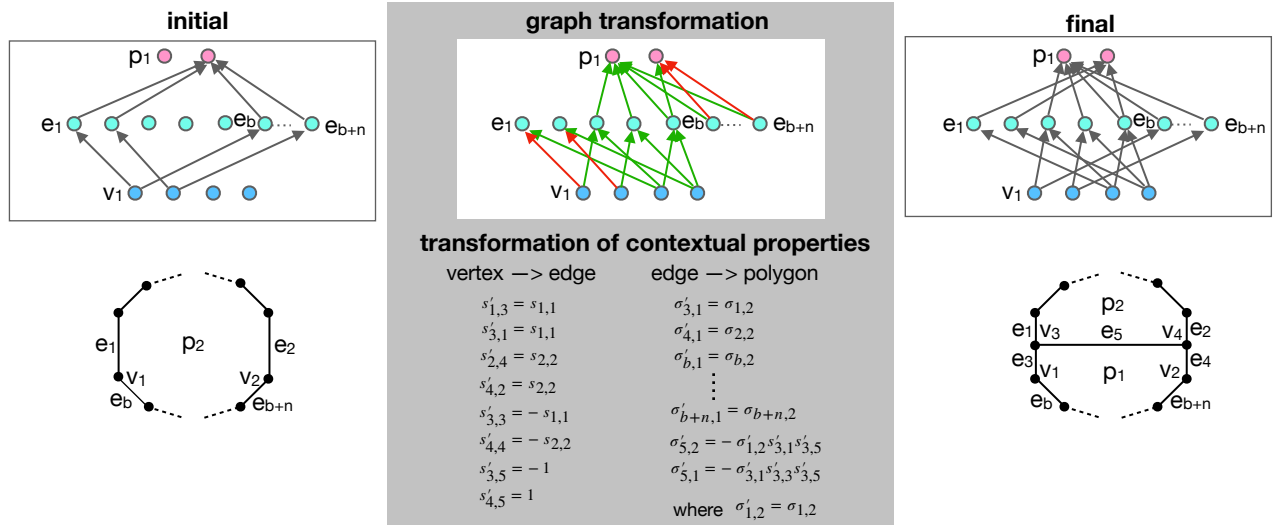


FIG. 2. **Geometry, topology and the graph transformation for a 2D cell division.** Subgraphs on the left and right show all involved components of a cell before and after cell division, respectively. All nodes follow the same color code as in Fig 1B. The subgraph in the middle column shows the graph transformation required to perform a cell division where deleted and newly created relationships are shown in red and green color, respectively. Additionally, the contextual properties of these newly created relationships are assigned at the bottom part of the middle column.

the locations of the new vertices, generated due to the intersection of these edges with e_5 , are calculated (see section A in SI). Given these new vertices, each intersected edge, e_1 and e_2 , generates pairs of daughter edges. For instance, the edge e_1 generates a pair e_1 and e_3 , whereas, the edge e_2 generates a pair e_2 and e_4 (Fig 2). After that, topological changes are performed in two consecutive steps as follows.

(i) **Pattern matching** retrieves a small subgraph from the entire graph of GVM. This subgraph contains all the relevant nodes involved in cell division and relationships between them. These data are found by traversing the entire graph database and filtering the results using specific graph-database queries and logical statements as described in more detail in [1].

For instance, given the intersected edge e_1 and one of its vertices v_1 , the pattern matching identifies the edge e_b which shares v_1 with e_1 and also belongs to polygon p_2 (Fig. 2). Similarly, we identify the edge, next to e_b in the opposite direction of e_1 , which also belongs to the polygon p_2 , eventually collecting all e_{b+i} edges of p_2 where $i = 0, 1, 2, \dots, n$, spanning between e_1 and the other intersected edge e_2 (Fig. 2). All the collected nodes and relationships between them construct the initial sub-graph representing the local network topology before the division (upper left panel of Fig. 2).

(ii) **Graph transformation** converts the initial sub-graph to perform cell division using a few relationship creations and deletions as shown in the upper-middle panel of Fig 2, where the deleted and newly created relationships are indicated by red- and green-colored arrows, respectively. For instance, at the vertex-edge level, rela-

tionships from v_1 to e_1 and v_2 to e_2 are deleted, whereas two relationships are created from v_1 to e_3 and from v_2 to e_4 . Furthermore, the vertices v_3 and v_4 , which become connected to the GVM graph through triple newly created relationships, are the intersections points of the division plane with the intersecting edges. The vertex v_3 is shared among e_1 , e_3 and e_5 while v_4 is the common vertex between e_2 , e_4 and e_5 . At the next hierarchical level, i.e., edge-polygon level, relationships between e_{b+i} and p_2 are deleted, but new relationships are established between e_{b+i} edges and one of the newly created polygons p_1 . Additionally, the two newly generated edges e_3 and e_4 create two new relationships to p_1 . Finally, relationships are created between e_5 and the two polygons p_1 and p_2 .

Contextual properties (i.e., signs) s and σ are assigned to all newly created relationships. Some of these properties are calculated from the relationships before division while some can be chosen arbitrarily. The equations in the middle panel of Fig. 2 summarize how s - and σ -values are calculated; the prime symbol indicates contextual properties after the division. For instance, $s'_{1,3}$, the sign of vertex v_1 in the context of edge e_3 is assigned the same sign as that of v_1 in the context of the edge e_1 before the division, since edge e_3 merely replaces the role of e_1 . In contrast, $s'_{3,5} = -1$ is arbitrarily chosen, since there is no restriction on vertices of the dividing edge e_5 . Among contextual properties that need to be calculated, the sign of e_5 in the context of p_2 , $\sigma'_{5,2}$ depends on three signs: (1) $\sigma'_{1,2}$, the sign of e_1 in the context of p_2 , (2) $s'_{3,1}$, the sign of v_3 in the context of e_1 and, (3) $s'_{3,5}$, the sign of v_3 in the context of e_5 . In short, $\sigma'_{5,2}$ receives the same

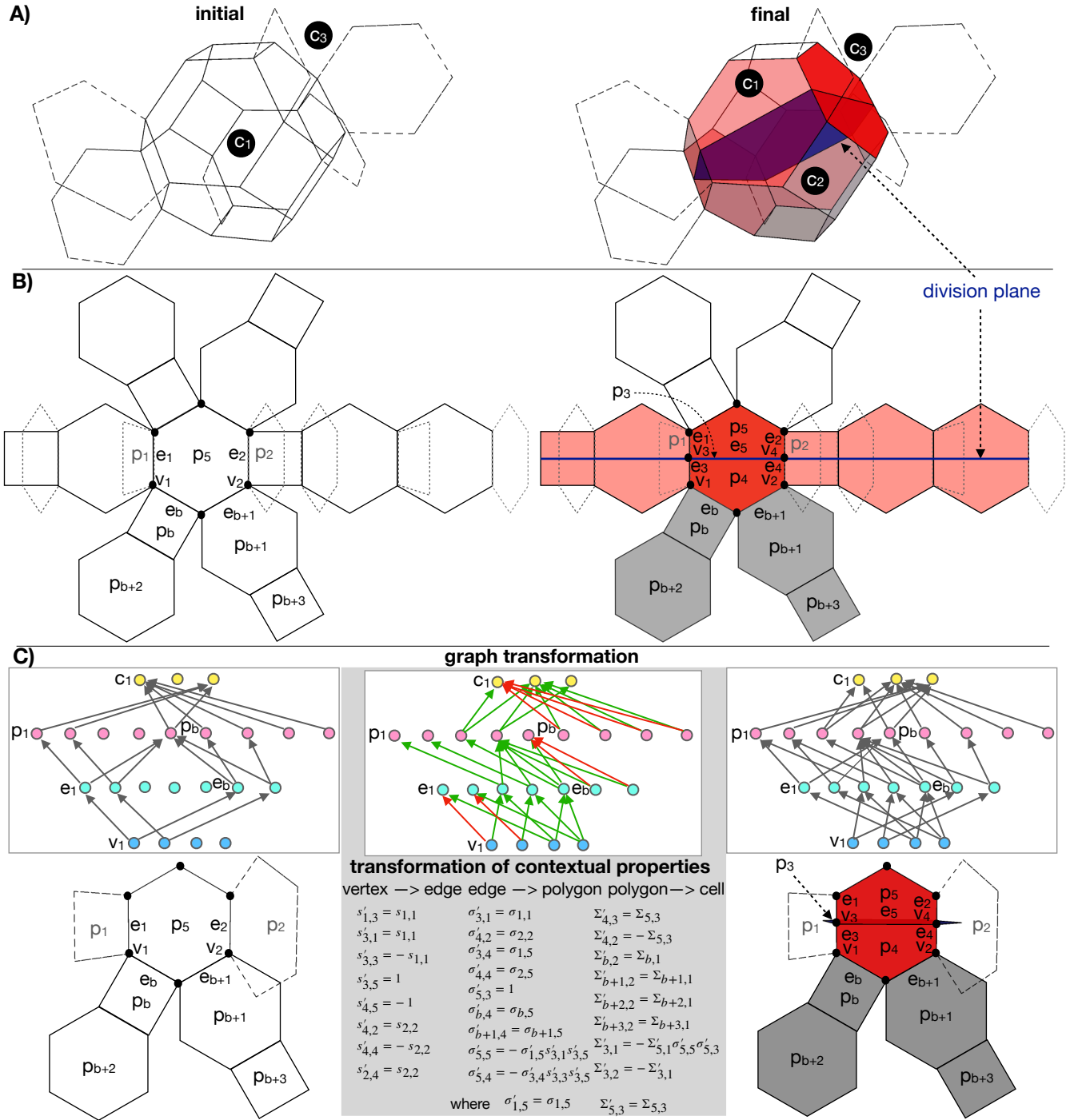


FIG. 3. Geometry, topology and the graph transformation for a 3D cell division. **A** The left and right columns show cells involved in cell division. Cell c_1 divides into two daughter cells, c_1 and c_2 . The division plane is dark blue, and new or intersected polygons are marked in red in the right column. One of these red polygons is randomly marked dark red. Each dark red polygon is shared with cell c_3 before division. Polygons above and below the red polygons are white and gray, respectively. **B** Polygons of c_1 are unwrapped and projected onto 2D before (left) and after (right) division, with the division plane as a straight line through the red polygons. Non- c_1 polygons are shown with dashed lines. **C** Subgraphs in the left and right columns highlight the components involved in division from the perspective of the dark red polygon. All nodes follow the same color code as in Fig. 1B. The middle column shows the graph transformation for cell division, with deleted and newly created relationships in red and green color, respectively. Contextual properties of new relationships are compactly shown at the bottom of the middle column.

or opposite sign of $\sigma'_{1,2}$ depending on the dissimilarity or similarity of $s'_{3,1}$ and $s'_{3,5}$, respectively.

Cell division in 3D cell aggregates

A 3D cell division follows a procedure similar to a 2D cell division. It begins by selecting an arbitrary plane of division and identifying all edges and polygonal faces of the dividing cell that it intersects; for instance, a blue-colored plane in Fig 3A passes through the center of the cell c_1 dividing it into two daughter cells, c_1 and c_2 . Additionally, the dividing plane intersects a few edges and polygonal faces, which are marked in red. For clarity, Fig. 3B shows all polygonal faces except for the dividing plane of c_1 and c_2 before and after the division, mapped onto a plane. In this 2D projection, the dividing plane appears as a blue-colored straight line dividing all intersected (red-colored) polygons.

We begin pattern matching by arbitrarily choosing one of the intersected polygons, such as the dark red-colored polygon p_5 in Fig. 3. This is followed by identifying all the nodes and relationships, involved in the transformation, using graph-database queries, similar to those in 2D. We note that the division of p_5 resembles the division of polygon p_2 in the 2D case (Fig. 2). In addition to the entities required for a 2D polygon division, a few additional entities are involved in 3D, e.g., two additional polygons, p_1 and p_2 , which share intersected edges, e_1 and e_2 , respectively, with p_5 and belong to the neighboring cell c_3 . On top of that, all intersected polygons, including p_5 , collectively constitute a patch (red-colored polygons in Fig. 3A and Fig. 3B) on cell c_1 . The remaining polygons of c_1 , positioned above and below this patch, marked in white and gray in Fig. 3, respectively, become part of two different daughter cells. However, only one set of polygons, those below the patch (p_{b+i} , where $i = 0, 1, 2 \dots$, etc.), marked in gray, undergoes a change in cell association, as the label c_1 of the dividing cell is reassigned to one of the daughter cells.

We construct the initial subgraph shown in the left panel of Fig. 3C by assembling all the nodes and their relationships identified during pattern matching of the chosen polygon. Note that the initial subgraph contains more nodes and relationships than the 2D cell division (Fig. 2) due to the involvement of additional polygons and cells, as described earlier. Next, similar to 2D cell division, the cell c_1 is divided by performing a graph transformation on the initial subgraph, which deletes and simultaneously creates a few relationships between nodes shown in the middle panel of Fig. 3C. After the graph transformation, contextual properties (signs), s , σ and Σ , are assigned to all newly generated relationships as illustrated at the bottom of the middle panel of Fig. 3C. A few additional relationships exist compared to the 2D cell division; for instance, the two daughter polygons, p_4 and p_5 receive the same sign that polygon p_5 had before division in the context of the cell c_3 , because the polygon p_5 is divided into two polygons without alter-

ing the adjacency to any previous cell. Similarly, p_4 is marked with the opposite sign of $\Sigma_{5,3}$ in the context of c_2 . However, the gray polygons in Fig. 3C, p_{b+i} , receive the same signs that they had before the division in the context of c_1 because the role of c_1 is merely replaced by c_2 during division. Additionally, sign of the dividing plane p_3 in the context of the daughter cell c_1 , $\Sigma'_{3,1}$ is based on three other signs including $\Sigma'_{5,1}$, $\sigma'_{5,5}$ and $\sigma'_{5,3}$ which ensures that $\Sigma'_{3,1}$ receives the same sign as $\Sigma'_{5,1}$ or the opposite based on whether the later two signs are different or identical.

Note that during the systematic application of pattern matching and graph transformation on each intersected polygon, components already assigned to daughter cells in previous steps remain unaltered, as they are no longer retrievable in the current step's pattern matching. For instance, the gray polygons assigned to daughter cell c_2 during the transformation of the first intersected polygon remain unchanged in subsequent transformations, since they are no longer part of the cell c_1 .

Generalization of cell division in 2D and 3D

During cell division in 3D, polygons intersected by the division plane get divided into pairs of polygons, just like in a 2D cell division. This indicates that, like in cell rearrangements [1], the same graph transformation describing cell division in 3D can be applied to a 2D polygonal tiling to describe a polygon division.

To investigate, we perform the same set of pattern matching of a 3D division on a 2D polygonal tiling illustrated by Fig. S2. Due to the absence of cells and a few accompanying polygons, only a part of the 3D subgraph is matched (Fig. S2A in SI). The unmatched nodes and relationships are shown in transparent shades. After relabelling p_5 and p_4 polygons in that subgraph by p_2 and p_1 , respectively, the resulting graph generates the same subgraph of a dividing polygon in 2D polygonal tiling (Fig. S2 in SI), thereby confirming that the graph transformation that performs a cell division in 2D is a subgraph of the more general 3D transformation.

Dynamics of growing cell aggregates

To showcase the ability of our method to simulate complex tissue mechanics, where cells both divide and rearrange, we use the extended GVM to simulate a periodic cell aggregate where cells divide randomly with a constant probability per time unit and rearrange in response to local shear stresses. The mechanical forces are encoded in our model through the potential energy

$$W = \sum_{\langle mn \rangle} \Gamma_{mn} A_{mn} + \kappa_V \sum_m (V_m - V_0)^2 . \quad (2)$$

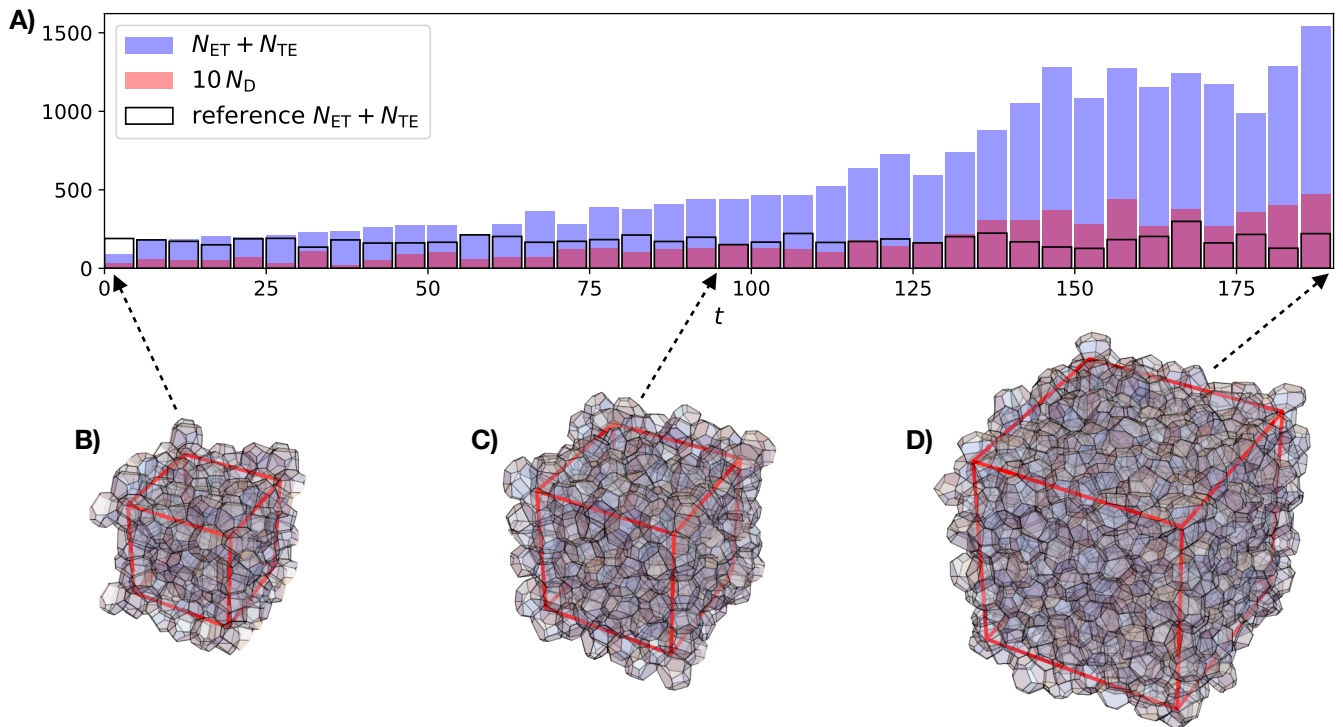


FIG. 4. **Topological transformations in a growing 3D cell aggregate.** **A** Solid blue and orange bars show the combined number of ET and TE transformations and cell divisions, respectively during the growth of a cell aggregate. The transparent bars with black borders represent a combined count of the ET and TE transformations in the absence of cell division. Each bar in this plot shows the number of topological transformations counted over a period of 5 units of time. **B-D** Initial, intermediate and final snapshots of the cell aggregate show a gradual increase in the cell aggregate's volume due to the appearance of daughter cells.

Here, A_{mn} and Γ_{mn} are the area of the interface between cells m and n and the effective surface tension on that interface, stemming from cell cortical tension and cell-cell adhesion [19–21]. The modulus κ_V in the second term in W is the cell-incompressibility modulus, which ensures that cell volumes V_m are roughly equal to the preferred volume V_0 .

The vertices of the cell aggregate follow overdamped dynamics as described by Eq. (1), where conservative forces are derived from the potential energy [Eq. (2)], whereas the active component describes active force dipoles acting along all edges. The active force exerted on vertex i reads

$$\mathbf{F}_i^{(a)} = - \sum_{mn} \gamma_{lmn}(t) \nabla_i L_{lmn}, \quad (3)$$

where lmn indicates an edge common among cells identified by the indices l , m , and n , with a length of L_{lmn} . The magnitudes of active force dipoles, $\gamma_{lmn}(t)$ fluctuate with time, obeying Ornstein-Uhlenbeck dynamics described by

$$\dot{\gamma}_{lmn}(t) = - \frac{1}{\tau_m} (\gamma_{lmn}(t) - \gamma_0) + \xi_{lmn}(t), \quad (4)$$

where τ_m is the relaxation time scale of this force towards a baseline value γ_0 [22, 23]. The $\xi_{lmn}(t)$ is a

Gaussian white noise with properties $\langle \xi_{lmn}(t) \rangle = 0$ and $\langle \xi_{lmn}(t) \xi_{opr}(t') \rangle = (2\sigma^2/\tau_m) \delta_{lo} \delta_{mp} \delta_{nr} \delta(t - t')$; σ^2 is the long-time variance of the force fluctuations.

We set up a simulation with a disordered cell aggregate of 90 cells (N_c) generated by adding spheres in a random sequence using the Voro++ package [24]. Additionally, we set $\sigma = 0.17$ close to the transition from a solid-like to a fluid-like behavior [1]. During the simulation, cells are randomly selected for division with a constant probability $p_d = 10^{-2}$ per unit time. In addition, TE and ET transformations are performed when edges become vanishingly short. Each selected cell grows its volume to $2V_0$ with a growth rate $g_t = 1$ before dividing into two daughter cells with preferred volume V_0 . We also slowly increase the simulation box's size to accommodate the growing cell's gradual volume increment. The simulation ends at time $t = 290$ time units and $N_c = 742$.

During the simulation, we counted the number of divisions and the combined number of ET and TE transformations using a window of 5 units of time, shown in orange- and blue-colored bars in Fig. 4A. We observe a systematic increase in the number of cell divisions with time. This increase occurs because cell division raises the total number of cells. Given the constant probability for cell division, a larger cell population leads to a

higher number of subsequent cell divisions. The increase of the number of cell divisions is also accompanied by the increase of ET and TE transformations. In contrast, we observe a significantly smaller number of TE and ET transformations, when the simulation begins with the final configuration of the first simulation but no cell divisions are allowed (transparent bars with black borders in Fig. 4A). These results show that the majority of ET and TE transformations, observed in the original simulation, are induced by local shear stresses caused by cell growth and division.

DISCUSSION

We implemented cell division within the framework of the GVM in both 2D and 3D cell aggregates. We found that analogous to the algorithm of cell rearrangements, introduced in [1], cell division can be performed in two steps: (a) pattern matching and (b) graph transformation. In pattern matching, all the elements involved in the division are identified, whereas in graph transformation, relationships among these identified elements are transformed. Initially, we defined the pattern matching and graph transformation for a polygon division in a 2D planar cellular tiling. Subsequently, we extended this approach to 3D by systematically applying a fixed set of pattern matching and graph transformations to the polygonal faces of a dividing cell that are intersected by the division plane in 3D. The graph transformations in both 2D and 3D are fundamentally similar, consisting of deleting certain existing relationships and creating new ones. Notably, the graph transformation required for 2D cell division appears to be a subset of that needed for 3D cell division. Moreover, we investigated the impact of cell division on cell rearrangements within a growing cell aggregate. Our results indicate cell divisions destabilise edges and polygons, promoting local rearrangements.

With the addition of cell division, GVM appears as a suitable tool for studying cell spheroids, which serve as an excellent model for investigating mechanistic evolution and characteristic shapes at various stages of tissue development. Additionally, GVM enables the exploration of the influence of cell-level effects on tissue-level phenomena, especially in bulk 3D tissue, which remains largely unexplored due to the computational hurdles. Given the critical role of cell division in tumor growth and cancer metastasis, incorporating cell division into GVM provides a straightforward method for advancing our understanding of the mechanical processes involved in tumor development and treatment.

- [1] T. Sarkar and M. Krajnc, Graph topological transformations in space-filling cell aggregates, *PLoS Computational Biology* **20**, e1012089 (2024).
- [2] H. Honda, Y. Ogita, S. Higuchi, and K. Kani, Cell movements in a living mammalian tissue: Long-term observation of individual cells in wounded corneal endothelia of cats, *Journal of Morphology* **174**, 25 (1982).
- [3] D. Weaire and N. Rivier, Soap, cells and statistics—random patterns in two dimensions, *Contemporary Physics* **25**, 59 (1984).
- [4] F. Graner, Y. Jiang, E. Janiaud, and C. Flament, Equilibrium states and ground state of two-dimensional fluid foams, *Physical Review E* **63**, 011402 (2000).
- [5] H. Honda, M. Tanemura, and T. Nagai, A three-dimensional vertex dynamics cell model of space-filling polyhedra simulating cell behavior in a cell aggregate, *Journal of theoretical biology* **226**, 439 (2004).
- [6] D. L. Weaire and S. Hutzler, *The physics of foams* (Oxford University Press, 1999).
- [7] B. I. Shraiman, Mechanical feedback as a possible regulator of tissue growth, *Proceedings of the National Academy of Sciences* **102**, 3318 (2005).
- [8] S. J. Day and P. A. Lawrence, Measuring dimensions: the regulation of size and shape, *Development* **127**, 2977 (2000).
- [9] I. Conlon and M. Raff, Size control in animal development, *Cell* **96**, 235 (1999).
- [10] N. Serrano and P. H. O’Farrell, Limb morphogenesis: connections between patterning and growth, *Current Biology* **7**, R186 (1997).
- [11] M. Milán, S. Campuzano, and A. García-Bellido, Cell cycling and patterned cell proliferation in the wing primordium of drosophila., *Proceedings of the National Academy of Sciences* **93**, 640 (1996).
- [12] J. A. Knoblich, Asymmetric cell division: recent developments and their implications for tumour biology, *Nature reviews Molecular cell biology* **11**, 849 (2010).
- [13] X. Morin and Y. Bellaïche, Mitotic spindle orientation in asymmetric and symmetric cell divisions during animal development, *Developmental cell* **21**, 102 (2011).
- [14] S. J. Morrison and J. Kimble, Asymmetric and symmetric stem-cell divisions in development and cancer, *nature* **441**, 1068 (2006).
- [15] L. Shahriyari and N. L. Komarova, Symmetric vs. asymmetric stem cell divisions: an adaptation against cancer?, *PloS one* **8**, e76195 (2013).
- [16] R. Alert and X. Trepat, Physical models of collective cell migration, *Annual Review of Condensed Matter Physics* **11**, 77 (2020).
- [17] A. G. Fletcher, M. Osterfield, R. E. Baker, and S. Y. Shvartsman, Vertex models of epithelial morphogenesis, *Biophysical journal* **106**, 2291 (2014).
- [18] S. Alt, P. Ganguly, and G. Salbreux, Vertex models: from cell mechanics to tissue morphogenesis, *Philosophical Transactions of the Royal Society B: Biological Sciences* **372**, 20150520 (2017).
- [19] J. Derganc, S. Svetina, and B. Žekš, Equilibrium mechanics of monolayered epithelium, *Journal of theoretical biology* **260**, 333 (2009).
- [20] M. L. Manning, R. A. Foty, M. S. Steinberg, and E.-M. Schoetz, Coaction of intercellular adhesion and cortical tension specifies tissue surface tension, *Proceedings of the National Academy of Sciences* **107**, 12517 (2010).
- [21] E. Hannezo, J. Prost, and J.-F. Joanny, Theory of epithe-

* tanmoy.sarkar@ijs.si

- lial sheet morphology in three dimensions, Proceedings of the National Academy of Sciences **111**, 27 (2014).
- [22] S. Curran, C. Strandkvist, J. Bathmann, M. de Gennes, A. Kabla, G. Salbreux, and B. Baum, Myosin II controls junction fluctuations to guide epithelial tissue ordering, *Developmental cell* **43**, 480 (2017).
- [23] M. Krajnc, Solid–fluid transition and cell sorting in epithelia with junctional tension fluctuations, *Soft Matter* **16**, 3209 (2020).
- [24] C. Rycroft, Voropp: A three-dimensional voronoi cell library in c++, *Chaos* **19**, 041111 (2009).

Graph polyhedral divisions in growing cell aggregates: Supplementary Information

Urban Železnik,^{1,2} Matej Krajnc,² and Tanmoy Sarkar^{2,*}

¹*Faculty of Mathematics and Physics, University of Ljubljana, Jadranska 19, SI-1000 Ljubljana, Slovenia*

²*Jožef Stefan Institute, Jamova 39, SI-1000 Ljubljana, Slovenia*

(Dated: August 15, 2024)

A. DETERMINING INTERSECTED EDGES AND VERTICES

To find intersecting edges of the dividing polygon p_2 , we inspect each of its edges, for instance, the edge e_1 connecting v_1 and v_u in Fig. S1A. We construct a pair of vectors \vec{R}_1 and \vec{R}_2 from the center of the polygon v_{CM} to the vertices v_1 and v_u , respectively. The projections of \vec{R}_1 and \vec{R}_2 onto the unit vector of the dividing plane \hat{n} are of opposite signs. Therefore, e_1 is marked as intersected. However, any non-intersecting edge shows projection values with identical signs.

After identifying the intersected edges, e_1 and e_2 (Fig. 2), we estimate the locations of intersecting points based on the coordinates of their constituting vertices, center of the polygon and \hat{n} . For instance, the location of the intersecting point v_3 (Fig. S1B) on the edge e_1 reads, $\vec{r}_1 + (\vec{r}_2 - \vec{r}_1) \frac{(\vec{r}_c - \vec{r}_1) \cdot \hat{n}}{(\vec{r}_2 - \vec{r}_1) \cdot \hat{n}}$, whereas, the location of v_4 on the edge e_2 is calculated by replacing v_1 , v_u and v_3 by v_2 , v'_u and v_4 , respectively. Here, v'_u is the vertex of e_2 other than v_2 .

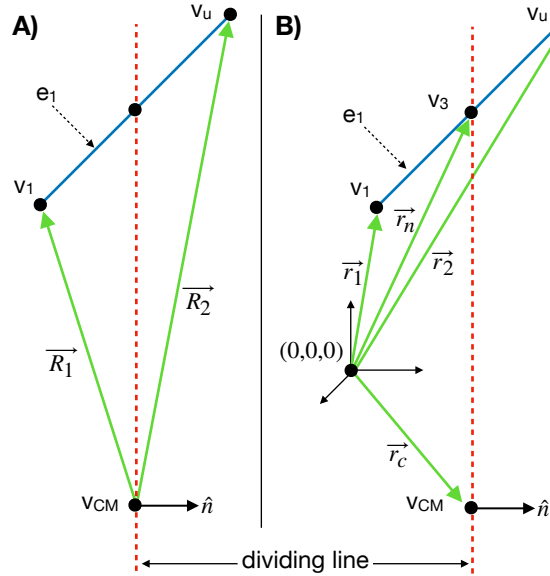


FIG. S1. Identification of an intersecting edge and estimation of the location of a new vertex due to intersection. The blue solid line represents the edge e_1 , while the red dotted line denotes the dividing plane. \hat{n} indicates the unit vector normal to the dividing plane. v_1 and v_u are the vertices defining edge e_1 . **A** The green vectors \vec{R}_1 and \vec{R}_2 extend from the center of mass of the polygon, v_{CM} , to vertices v_1 and v_u , respectively. **B** Vectors \vec{r}_1 , \vec{r}_2 , \vec{r}_n , and \vec{r}_c originate from the coordinate system's origin and point to vertices v_1 , v_u , v_3 , and v_{CM} , respectively. Vertex v_3 is the newly generated vertex resulting from the intersection of the dividing plane with edge e_1 .

* tanmoy.sarkar@ijs.si

B. SIMILARITIES BETWEEN 2D AND 3D CELL DIVISION

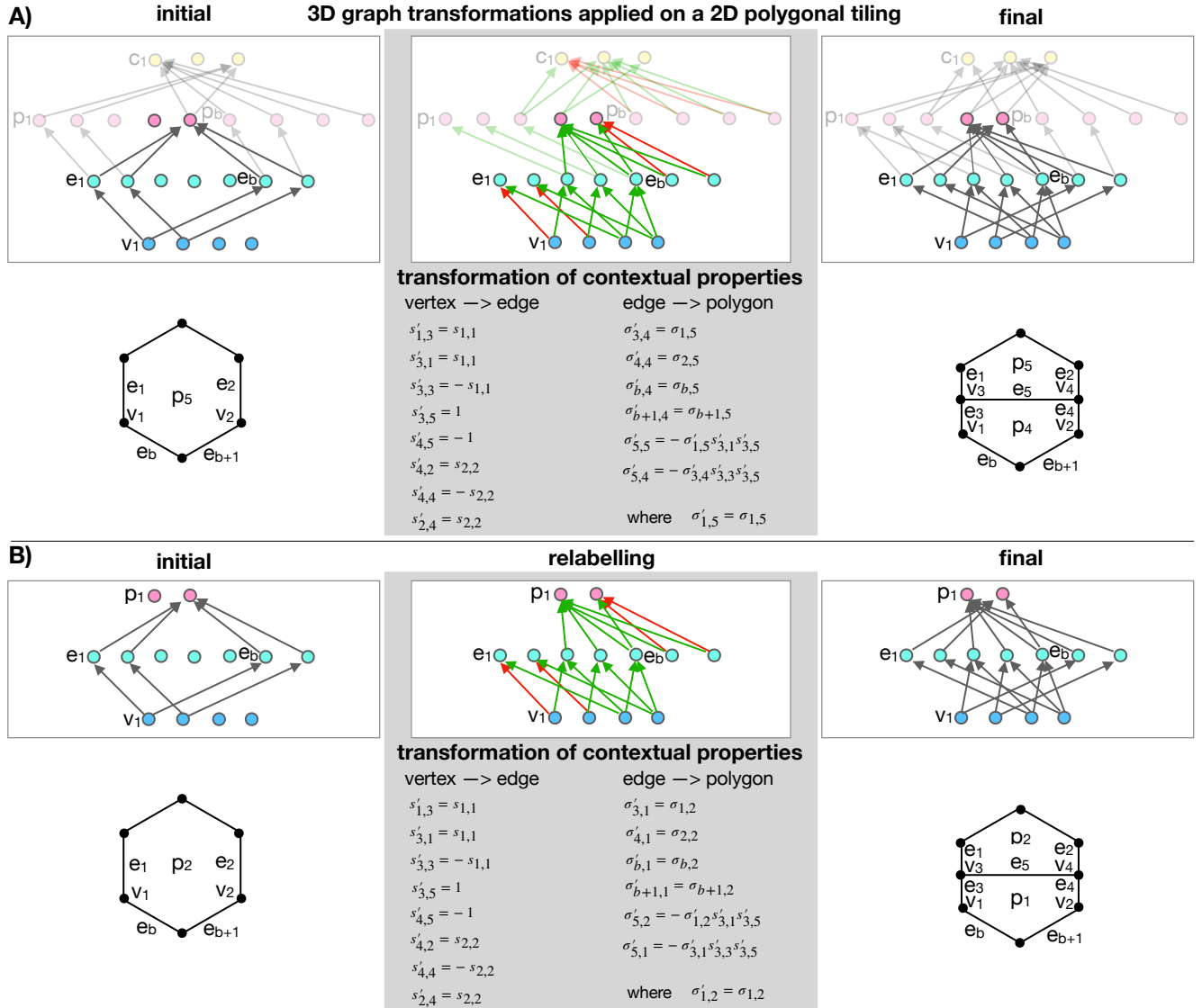


FIG. S2. **A** A set of graph transformations in 3D reduces to a 2D cell division when applied on planar polygonal tiling. **A** The graph transformation for dividing a polygonal face during 3D cell division (Fig. 3) is applied on a 2D planar polygonal tiling. In the initial (left), final (right), and transformation subgraph (middle column), some nodes and relationships are shown as transparent, indicating unmatched elements due to their absence in the 2D packing. **B** After relabelling the polygon nodes, we observe that these three subgraphs exactly match the graph in the context of dividing a planar polygon.

C. GROWTH DYNAMICS

The supplemental movie file, growth-movie.mp4, illustrates the dynamic process of cellular aggregate growth from the original simulation presented in Fig. 4. This movie demonstrates cell divisions and rearrangements within the aggregate throughout the simulation.